



Article

Pinostrobin Suppresses the α -Melanocyte-Stimulating Hormone-Induced Melanogenic Signaling Pathway

Athapaththu Mudiyansele Gihan Kavinda Athapaththu ^{1,†}, Sobarathne Senel Sanjaya ^{1,†}, Kyoung Tae Lee ², Wisurumuni Arachchilage Hasitha Maduranga Karunarathne ^{1,3}, Yung Hyun Choi ⁴, Sung-Pyo Hur ^{1,‡} and Gi-Young Kim ^{1,*}

¹ Department of Marine Life Science, Jeju National University, Jeju 63243, Republic of Korea

² Forest Bioresources Department, Forest Microbiology Division, National Institute of Forest Science, Suwon 16631, Republic of Korea

³ Department of Biosystems Technology, Faculty of Technology, University of Ruhuna, Matara 81000, Sri Lanka

⁴ Department of Biochemistry, College of Korean Medicine, Dong-Eui University, Busan 47227, Republic of Korea

* Correspondence: immunkim@jejunu.ac.kr

† These authors contributed equally to this work.

‡ These authors contributed equally to this work.

Abstract: Pinostrobin is a dietary flavonoid found in several plants that possesses pharmacological properties, such as anti-cancer, anti-virus, antioxidant, anti-ulcer, and anti-aromatase effects. However, it is unclear if pinostrobin exerts anti-melanogenic properties and, if so, what the underlying molecular mechanisms comprise. Therefore, we, in this study, investigated whether pinostrobin inhibits melanin biosynthesis in vitro and in vivo, as well as the potential associated mechanism. Pinostrobin reduced mushroom tyrosinase activity in vitro in a concentration-dependent manner, with an IC₅₀ of 700 μ M. Molecular docking simulations further revealed that pinostrobin forms a hydrogen bond, as well as other non-covalent interactions, between the C-type lectin-like fold and polyphenol oxidase chain, rather than the previously known copper-containing catalytic center. Additionally, pinostrobin significantly decreased α -melanocyte-stimulating hormone (α -MSH)-induced extracellular and intracellular melanin production, as well as tyrosinase activity, in B16F10 melanoma cells. More specifically, pinostrobin inhibited the α -MSH-induced melanin biosynthesis signaling pathway by suppressing the cAMP–CREB–MITF axis. In fact, pinostrobin also attenuated pigmentation in α -MSH-stimulated zebrafish larvae without causing cardiotoxicity. The findings suggest that pinostrobin effectively inhibits melanogenesis in vitro and in vivo via regulation of the cAMP–CREB–MITF axis.

Keywords: pinostrobin; melanogenesis; tyrosinase; α -MSH



Citation: Athapaththu, A.M.G.K.; Sanjaya, S.S.; Lee, K.T.; Karunarathne, W.A.H.M.; Choi, Y.H.; Hur, S.-P.; Kim, G.-Y. Pinostrobin Suppresses the α -Melanocyte-Stimulating Hormone-Induced Melanogenic Signaling Pathway. *Int. J. Mol. Sci.* **2023**, *24*, 821. <https://doi.org/10.3390/ijms24010821>

Academic Editor: Tack-Joong Kim

Received: 16 November 2022

Revised: 27 December 2022

Accepted: 27 December 2022

Published: 3 January 2023



Copyright: © 2023 by the authors. Licensee MDPI, Basel, Switzerland. This article is an open access article distributed under the terms and conditions of the Creative Commons Attribution (CC BY) license (<https://creativecommons.org/licenses/by/4.0/>).

1. Introduction

Once melanin is synthesized in melanocytes, it is incorporated into the melanosome, an organelle that is transported to adjacent keratinocytes, resulting in melanin distribution [1]. Melanin, and in particular, eumelanin, protects human skin from ultraviolet radiation (UVR)-induced DNA and skin damage by absorbing UVR and scavenging UVR-induced reactive oxygen species (ROS) [2]. Hence, melanin is thought to serve as the primary photoprotective pigment that suppresses UVR-induced oxidative stress and damage. However, the unusual accumulation of melanin also causes dermatological disorders, including melasma, wrinkling, senile lentiginos, and skin cancers [3–5]. Hence, identification and characterization of anti-melanogenic compounds has attracted considerable attention [6,7].

Tyrosinase plays an important role in increasing melanin biosynthesis through hydroxylation of tyrosine into dihydroxyphenylalanine (DOPA), followed by further oxidation into dopaquinone, which is the precursor for melanin via cysteinyl-DOPA and dopachrome, respectively [8,9]. Given that tyrosinase has been recognized as a major target molecule for

the inhibition of melanin biosynthesis, many antagonists have been developed and applied clinically [2]. Tyrosinase is a di-copper oxidase in which six histidine residues surround two copper ions in its catalytically active site [10]. Goldfeder et al. [11] reported that the main substrates of tyrosinase fit in the active site, whereas the presence of Zn^{2+} ions forces out the Cu^{2+} ions, effectively inhibiting the catalytic activity. In this way, many flavonoids competitively target the active site of tyrosinase, thereby inhibiting its activity [8,9]. Accordingly, competitive inhibitors targeting tyrosinase may represent an excellent strategy for inhibiting melanin biosynthesis.

UVR increases the expression of α -melanocyte-stimulating hormone (α -MSH) in keratinocytes, which binds to the melanocortin 1 receptor (MC1R) in melanocytes and promotes melanin biosynthesis [12]. Binding of α -MSH to MC1R primarily activates adenylyl cyclase (AC), which increases intracellular cyclic 3',5'-cyclic adenosine monophosphate (cAMP) levels and consequently stimulates protein kinase A (PKA) [13]. Subsequently, cAMP-responsive element-binding protein (CREB) is phosphorylated, which, together with CBP/p300, enhances the expression of microphthalmia-related transcription factor (MITF), a main regulator of tyrosinase expression [14]. Therefore, targeting the α -MSH-mediated signaling pathway may inhibit melanin biosynthesis by suppressing tyrosinase expression.

Pinostrobin (Figure 1A) is a natural flavonoid found in various plants, such as the leaves of *Cajanus cajan* (L.) Millsp and the rhizomes of *Boesenbergia rotunda* (L.). Pinostrobin possesses a broad spectrum of pharmacological activities, including anti-cancer [15,16], antioxidant [17], anti-inflammatory [18,19], and anti-virus properties [20]. In fact, El-Nashar et al. [21] recently reported that pinostrobin, isolated from Egyptian propolis, effectively reduces in vitro mushroom tyrosinase activity. However, there is currently a dearth of data regarding the anti-melanogenic effects of pinostrobin. Therefore, in this study, we investigated whether pinostrobin downregulates melanogenesis in B16F10 melanoma cells and zebrafish larvae by inhibiting the melanogenic signaling.

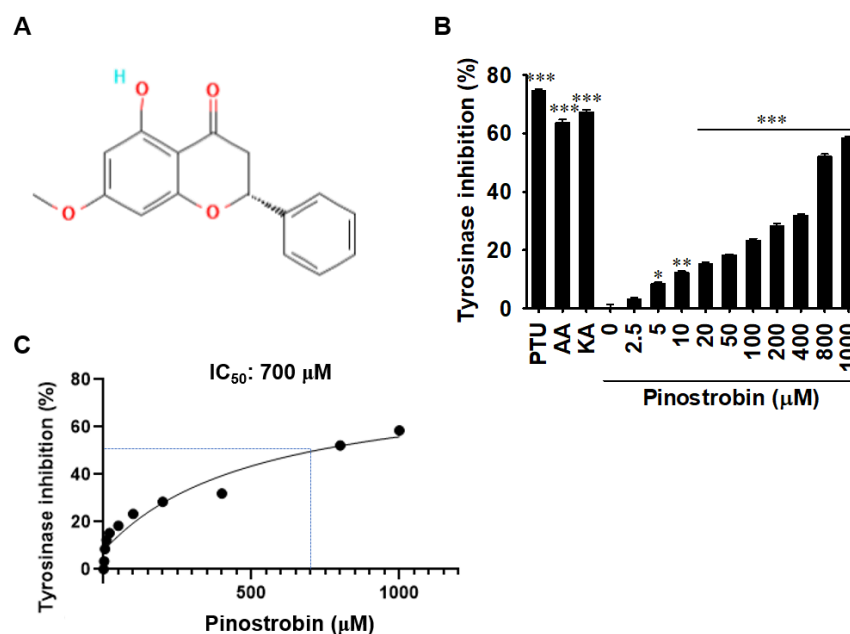


Figure 1. Pinostrobin inhibits in vitro mushroom tyrosinase activity. (A) Chemical structure of pinostrobin. (B) In vitro mushroom tyrosinase activity, as assessed by quantifying dopaquinone levels, following treatment with pinostrobin (0–1000 μ M), phenylthiourea (PTU, 250 nM), ascorbic acid (AA, 500 μ M), and kojic acid (KA, 25 μ M). Data are reported as the mean \pm SE. * $p < 0.05$, ** $p < 0.01$, and *** $p < 0.001$ vs. untreated control. (C) Pinostrobin concentration required for 50% inhibition (IC_{50}).

2. Results

2.1. Pinostrobin Inhibits In Vitro Mushroom Tyrosinase Activity

As tyrosinase is a rate-limiting enzyme in melanogenesis [8,9], we investigated whether pinostrobin negatively regulates mushroom tyrosinase activity in vitro. As expected, the tyrosinase inhibitors phenylthiourea (PTU), ascorbic acid (AA), and kojic acid (KA) significantly inhibited mushroom tyrosinase activity by $74.7\% \pm 0.6\%$, $63.8\% \pm 1.0\%$, and $67.4\% \pm 0.6\%$, respectively (Figure 1B). Meanwhile, as the concentration of pinostrobin gradually increased, in vitro mushroom tyrosinase activity was inhibited, and 1000 μM pinostrobin exhibited the strongest inhibitory effect ($58\% \pm 0.6\%$). In addition, the concentration required for 50% inhibition (IC_{50}) was confirmed to be approximately 700 μM (Figure 1C). Collectively, these data suggest that pinostrobin directly inhibits tyrosinase activity in vitro at high concentrations.

2.2. Pinostrobin Non-Competitively Binds to Tyrosinase

Whether pinostrobin inhibits in vitro mushroom tyrosinase activity by competing with its substrate was analyzed using a protein–ligand docking simulation. Using SwissDock, 34 clusters in which pinostrobin binds to mushroom tyrosinase were identified (Figure 2A). The major binding site was identified (Figure 2A 'a'), to which approximately 50% of clusters (0, 1, 3, 4, 8, 13, 17, 20, 21, 22, 23, 24, 27, 28, 30, and 34) were bound (Supplementary Table S1). Meanwhile, clusters 2, 6, 9, 14, 18, 19, 31, and 33 were bound to alternative binding site (Figure 2A 'b'), where the second highest binding force was observed. Additionally, four minor pinostrobin-binding sites were identified (Figure 2A 'c–f'). The 3D conformation (Figure 2B) and ribbon structure (Figure 2C) also showed the major pinostrobin binding site and the active site of tyrosinase containing Cu^{2+} ions. In particular, pinostrobin formed a hydrogen bond with TYR98 (HN) in the light chain (L, lectin-like fold protein) at a distance of 2.4769 Å (Figure 2D). In addition to the conventional hydrogen bond with TYR98, the 2D interaction diagram showed the formation of carbon hydrogen bonds (THR324), alkyl or π -alkyl bonds (TYR78, ILE324, and PRO338), and many van der Waals interactions with the surrounding amino acids (Figure 2E). These results indicate that pinostrobin does not compete with substrates at the active site of tyrosinase but rather primarily binds to heavy (H, polyphenol oxidase) and light chains.

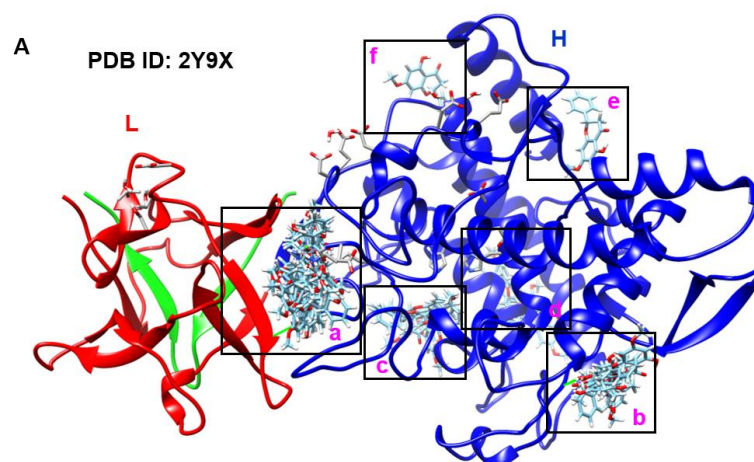


Figure 2. Cont.

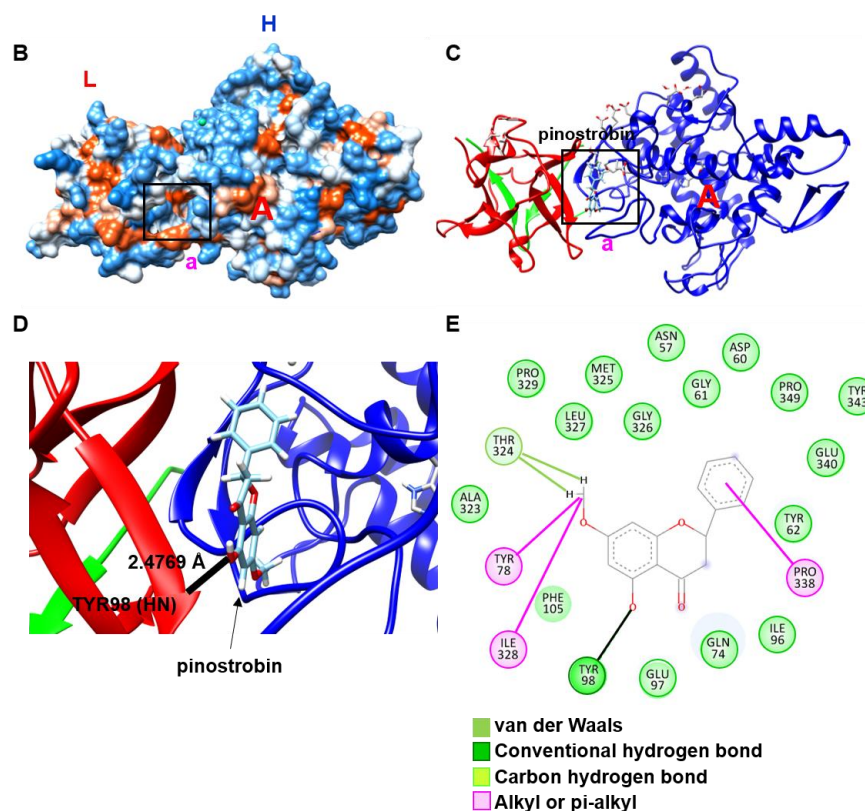


Figure 2. Pinostrobin non-competitively binds to mushroom tyrosinase (PDB ID: 2Y9X). (A) A total of 36 binding clusters of pinostrobin to mushroom tyrosinase were obtained from SwissDock. a, binding site for clusters 0, 1, 4, 8, 13, 17, 20, 21, 22, 23, 24, 27, 28, 30, and 34; b, binding site for clusters 2, 6, 9, 14, 18, 19, 31, and 33; c, binding site for clusters 7, 11, 25, 26, 32; d, binding site for clusters 12, 15, and 29; e, binding site for clusters 5 and 16; f, binding site for cluster 10. L, light chain (lectin-like fold protein); H, heavy chain (polyphenol oxidase). (B) The 3D conformation and (C) ribbon model how molecular docking site of pinostrobin (pink 'a') with mushroom tyrosinase. Red 'A' represents an active site of mushroom tyrosinase. (D) Enlarged binding site of pinostrobin with mushroom tyrosinase. A black line shows a hydrogen bond between pinostrobin and mushroom tyrosinase. (E) The 2D interaction poses of pinostrobin with mushroom tyrosinase.

2.3. Pinostrobin Concentrations above 100 μM Are Weakly Cytotoxic

To investigate whether pinostrobin is cytotoxic, B16F10 melanoma cells were treated with pinostrobin (0–1000 μM) for 72 h, and cytotoxicity was evaluated based on morphological changes and MTT assay. Observation under a phase-contrast microscope showed that pinostrobin treatment did not induce any morphological changes in the cells (Figure 3A). However, the MTT assay showed that treatment with pinostrobin at concentrations ≥ 100 μM markedly decreased the relative cell viability after 24 h ($77.3\% \pm 1.0\%$ and $54.3\% \pm 0.5\%$ at 100 and 200 μM , respectively); the inhibitory effect became stronger after 48 h ($68.3\% \pm 1.1\%$ and $49.2\% \pm 0.2\%$ at 100 and 200 μM , respectively) and 72 h ($39.6\% \pm 0.1\%$ and $30.6\% \pm 0.2\%$ at 100 and 200 μM , respectively; Figure 2B).

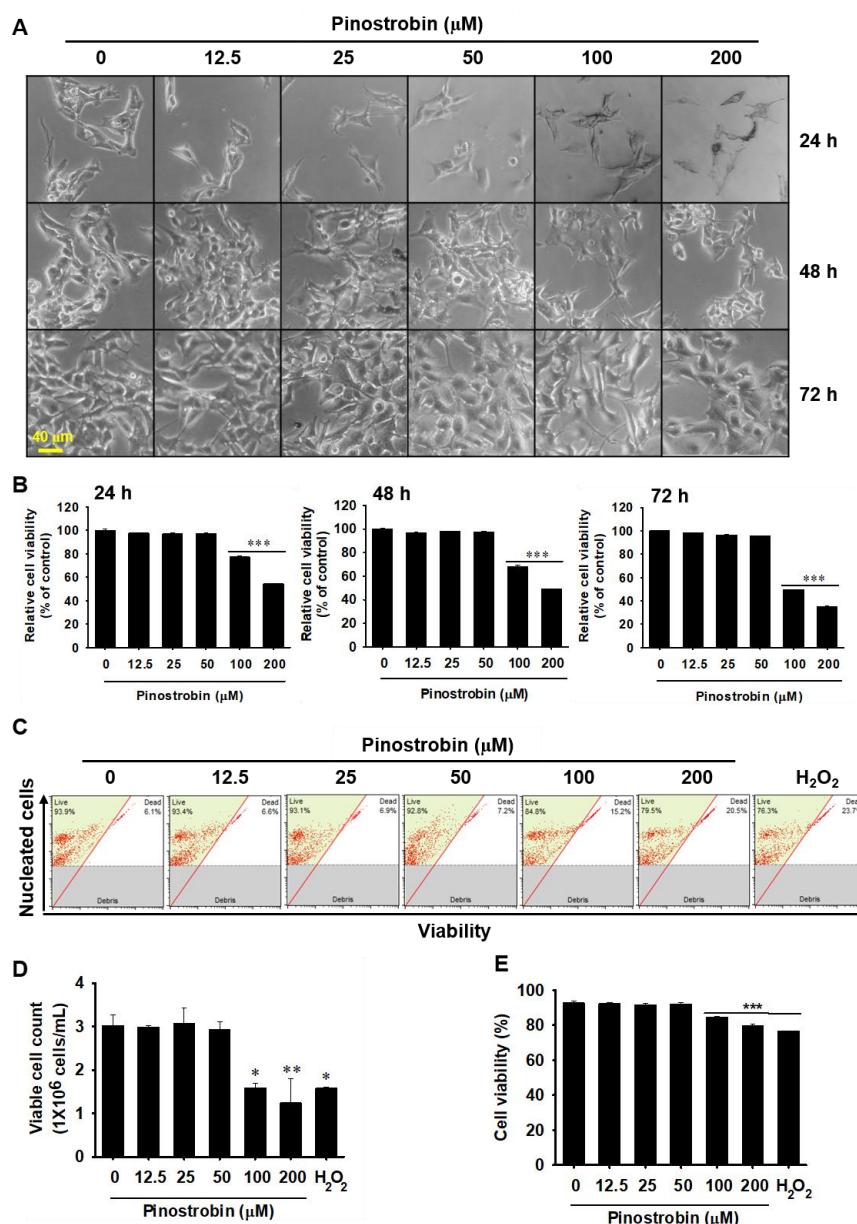


Figure 3. Pinostrobin at concentrations below 50 μM is not toxic to B16F10 melanoma cells. B16F10 cells were treated with pinostrobin (0–200 μM) for 72 h. (A) Microscopic images captured every 24 h. Scale bar = 40 μm . (B) Relative cell viability presented relative to the values of the untreated cells. (C) Treatment of cells with pinostrobin for 72 h. The cells were stained with a Muse Cell Count and Viability Kit. (D) Viable cell counts; (E) cell viability. Data are reported as mean \pm SE. * $p < 0.05$, ** $p < 0.01$, and *** $p < 0.001$ vs. untreated cells.

To confirm whether pinostrobin influences cell death, flow cytometric analysis was performed (Figure 3C). Consistent with the MTT assay results, 72 h after pinostrobin treatment, when compared to untreated cells ($(3.0 \pm 0.2) \times 10^6$ cells/mL), 100 μM and 200 μM pinostrobin significantly reduced viable cell counts ($(1.6 \pm 0.1) \times 10^6$ cells/mL and $(1.2 \pm 0.6) \times 10^6$ cells/mL, respectively; Figure 3D). Moreover, the viable cell population slightly decreased to $85.8\% \pm 0.2\%$ and $80.9\% \pm 2.4\%$ at 100 and 200 μM pinostrobin, respectively, compared to that in untreated cells ($92.8\% \pm 0.2\%$; Figure 3E). H₂O₂ treatment for 24 h also significantly decreased viable cell counts $(1.6 \pm 0.6) \times 10^6$ cells/mL and the viable cell population ($76.7\% \pm 0.8\%$). However, pinostrobin at concentrations ≤ 50 μM had no effect on cell growth. These data indicate that pinostrobin at concentrations below 50 μM has no direct cytotoxic effects.

2.4. Pinostrobin Decreases Melanin Production and Intracellular Tyrosinase Activity

To investigate the anti-melanogenic effect of pinostrobin, α -MSH-stimulated B16F10 melanoma cells were treated with various concentrations of pinostrobin (0–50 μ M) for 48 h, and the melanin content was measured in the extracellular and intracellular compartments. The degree of indirect melanin biosynthesis was assessed based on the change in media color during cell culture; a dark brown color indicates the presence of melanin. The results show a clear increase in melanin following treatment with α -MSH, which gradually decreased upon pinostrobin treatment (Figure 4A). Additionally, α -MSH significantly increased the extracellular and intracellular melanin contents to approximately 172% (Figure 4B) and 186% (Figure 4C), respectively. Meanwhile, pinostrobin downregulated α -MSH-induced extracellular and intracellular melanin content in a concentration-dependent manner. Pinostrobin (50 μ M) also decreased α -MSH-induced intracellular tyrosinase activity from approximately 160% to 113% (Figure 4D). In contrast, the group treated with only 50 μ M pinostrobin, without α -MSH pretreatment, exhibited melanin content and tyrosinase activity similar to those of untreated cells. These data indicate that pinostrobin inhibits extracellular and intracellular melanin production, as well as tyrosinase activity.

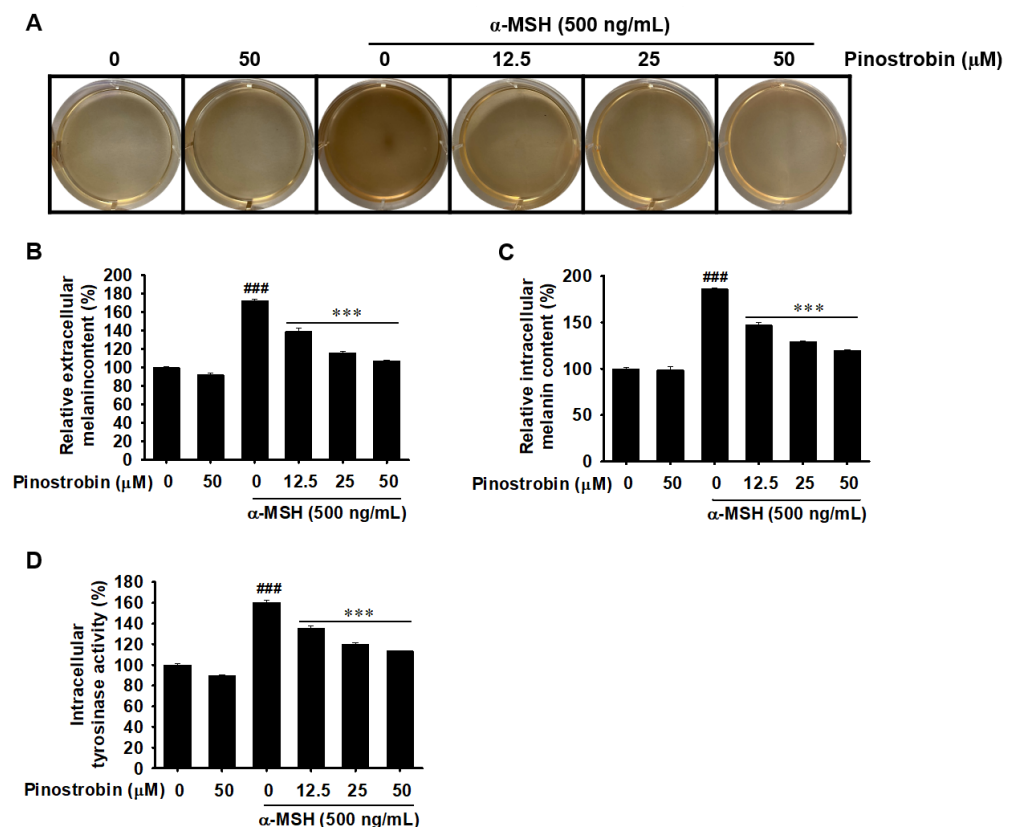


Figure 4. Pinostrobin decreases α -melanocyte-stimulating hormone (α -MSH)-stimulated melanin production and intracellular tyrosinase activity. B16F10 melanoma cells were stimulated with 500 ng/mL α -MSH for 24 h followed by treatment with pinostrobin (0–50 μ M) for 48 h. (A) The color change of each well. (B) Extracellular melanin content following stimulation with or without α -MSH and treatment with pinostrobin. (C) Intracellular melanin content following stimulation with or without α -MSH and treatment with pinostrobin. (D) Intracellular tyrosinase activity following treatment with B16F10 cells with pinostrobin and stimulation with or without α -MSH. The data are represented as mean \pm SE. ### $p < 0.001$ vs. untreated cells; *** $p < 0.001$ vs. α -MSH-treated cells.

2.5. Pinostrobin Inhibits cAMP, p-CREB, MITF, and Tyrosinase Expression in α -MSH-Stimulated B16F10 Melanoma Cells

To elucidate the mechanism by which pinostrobin inhibits the α -MSH-induced melanogenic signaling pathway, we measured cAMP levels induced by the binding of

α -MSH to MC1R. As shown in Figure 5A, pinostrobin significantly downregulated the increase in cAMP levels induced by α -MSH from 421.7 ± 14.3 pg/mL to 231.0 ± 21.7 pg/mL, 144.4 ± 5.1 pg/mL, and 96.9 ± 3.4 pg/mL at 12.5, 25, and 50 μ M, respectively. Considering that upregulation of intracellular cAMP is directly associated with CREB phosphorylation, we also evaluated the effect of pinostrobin on CREB phosphorylation. α -MSH markedly increased the expression of phosphorylated CREB (p-CREB), whereas pinostrobin decreased p-CREB expression in a concentration-dependent manner (Figure 5B). Additionally, α -MSH noticeably upregulated MITF and tyrosinase at both the translational (Figure 5C) and transcriptional (Figure 5D) levels whereas pinostrobin reduced α -MSH-induced MITF and tyrosinase expression at both levels. These results indicate that pinostrobin inhibits the melanogenic signaling pathway by suppressing the cAMP–CREB–MITF–tyrosinase axis.

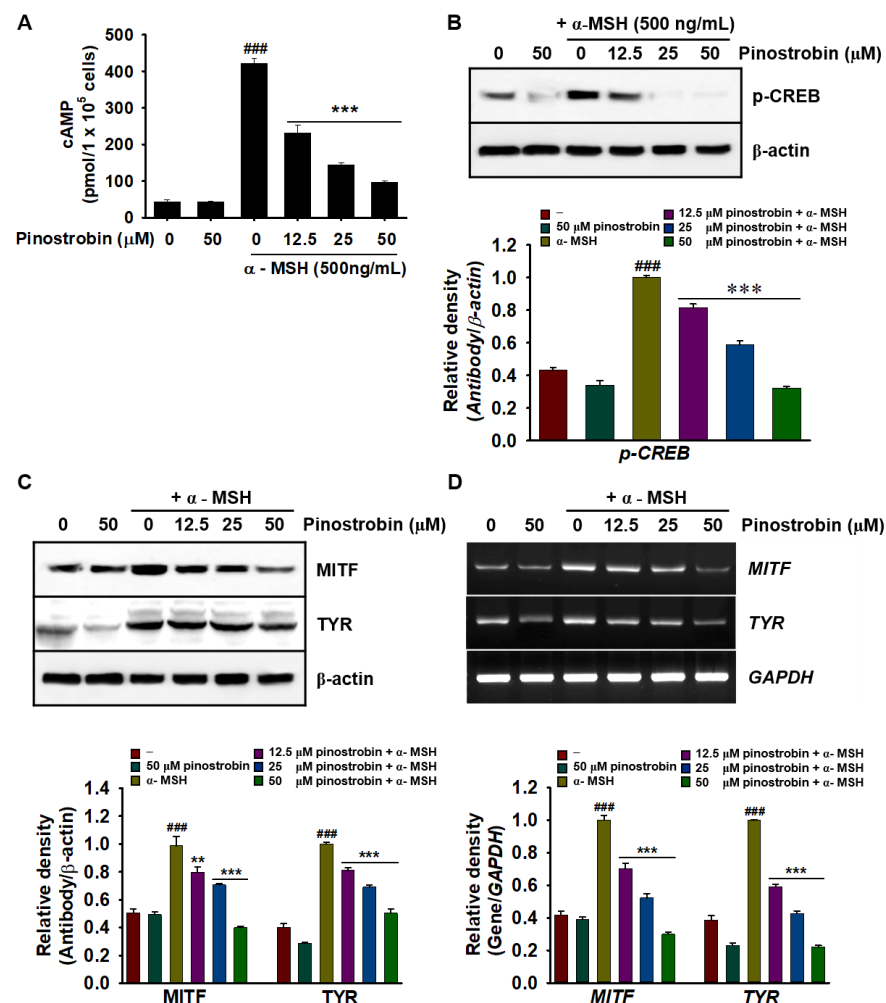


Figure 5. Pinostrobin inhibits α -melanocyte-stimulating hormone (α -MSH)-induced melanogenic signaling pathway. (A) Intracellular cAMP levels of B16F10 melanoma cells following pretreatment with IBMX for 10 min and treatment with pinostrobin in the presence or absence of α -MSH. (B,C) Protein abundance of phospho-cAMP-responsive element-binding protein (p-CREB), microphthalmia-related transcription factor (MITF), and tyrosinase (TYR) in B16F10 melanoma cells exposed to α -MSH and subsequently treated with pinostrobin. (D) Expression of *MITF* and *TYR* in B16F10 melanoma cells exposed to α -MSH and subsequently treated with pinostrobin. The data are represented as mean \pm SE. ### $p < 0.001$ vs. untreated cells; ** $p < 0.01$ and *** $p < 0.001$ vs. α -MSH-stimulated cells.

2.6. Pinostrobin Inhibits Melanin Pigmentation in Zebrafish Larvae

To further evaluate the anti-melanogenic activity of pinostrobin, we treated α -MSH-stimulated zebrafish larvae with pinostrobin and quantified subsequent melanogenesis.

As expected, pinostrobin markedly decreased α -MSH-induced melanin pigmentation in zebrafish larvae in a concentration-dependent manner (Figure 6A). Pinostrobin at 25 μ M inhibited α -MSH-induced melanin pigmentation in untreated zebrafish larvae (Figure 6B). To determine whether pinostrobin exerted cardiotoxicity in zebrafish larvae, we monitored the heart rate and found that zebrafish larvae treated with pinostrobin did not show any apparent difference compared to that in the untreated larvae (Figure 6C). Furthermore, neither morphological malformations nor mortality of the larvae were observed following treatment with pinostrobin for 48 h. These results suggest that pinostrobin is also a potent inhibitor of melanogenesis in vivo.

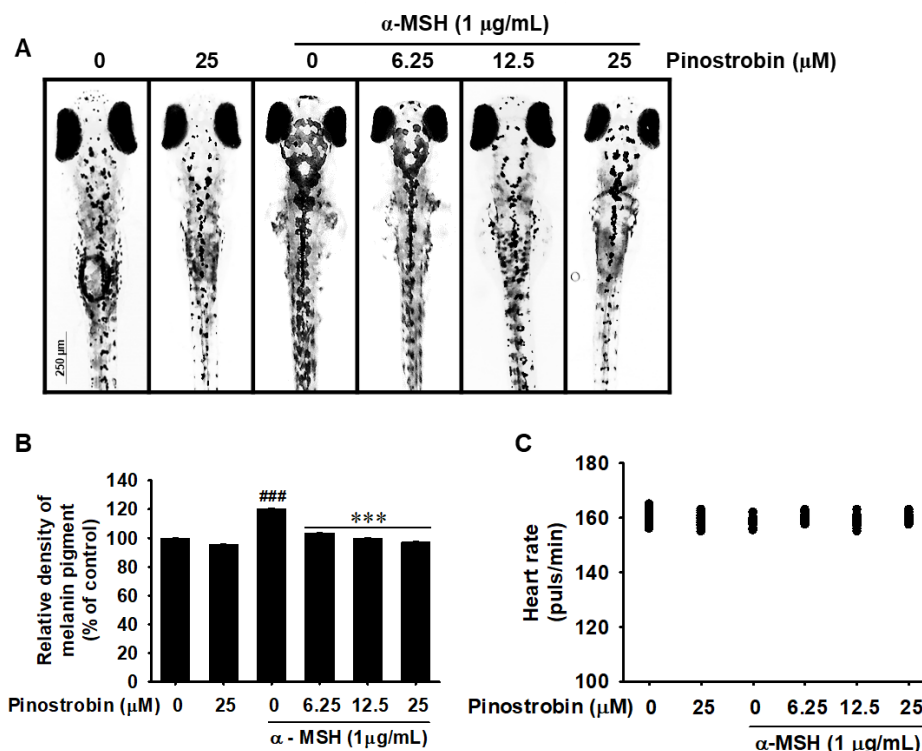


Figure 6. Pinostrobin inhibits melanin biosynthesis in zebrafish larvae. Zebrafish larvae at 2 dpf treated with phenylthiourea (PTU, 200 μ M) and stimulated with α -melanocyte-stimulating hormone (α -MSH, 1 μ g/mL). (A) Microscopic evaluation of zebrafish larvae pigmentation (40 \times). (B) Relative melanin pigment density. Scale bar = 250 μ m. (C) Average heart rate of zebrafish larvae ($n = 20$). Data are reported as the mean \pm SE. ^{###} $p < 0.001$ vs. untreated zebrafish larvae; ^{***} $p < 0.001$ vs. α -MSH-stimulated zebrafish larvae.

3. Discussion

UV exposure promotes α -MSH expression in keratinocytes, which stimulates the melanogenic signaling pathway by binding to MC1R in melanocytes [1,22]. The melanin produced by melanocytes spreads to the epidermis via keratinocytes and protects cells against UV-induced ROS stress and apoptosis [2,23]. However, abnormal hyperpigmentation creates skin darkness, such as spots or patches, by increasing melanin production when skin cells are severely damaged [24]. In addition to skin injury, accumulated melanin also induces acquired hyperpigmentation disorders, including metabolic, endocrine, and nutritional disorders [25]. Therefore, many drugs that can effectively inhibit tyrosinase activity with few side effects have been developed and are currently being used in clinical practice [26]. In this respect, many flavonoids that target tyrosinase have been evaluated [21]. Although several previous studies have demonstrated that pinostrobin inhibits tyrosinase activity in vitro [21,27], the exact molecular mechanism has not been studied. In this study, we determined that pinostrobin inhibits α -MSH-induced melanogenic activity. Contrary to our findings, Yoon et al. recently confirmed that pinostrobin stimulates spontaneous intra-

cellular melanin content and tyrosinase activity accompanied by high expression of MITF and CREB [28]. The authors also showed no cytotoxic effect in pinostrobin-treated B16F10 cells using MTT assay. In our study, high concentrations of pinostrobin significantly decreased relative cell viability using the MTT assay (precisely, it shows NADPH-dependent cellular oxidoreductase enzyme activity, not viability), as well as total cell numbers using flow cytometry; however, flow cytometry data also showed that pinostrobin slightly downregulated viable cell population, which indicates that pinostrobin disturbs or arrests the cell cycle, and does not show strong cytotoxicity, as reported previously [29]. It is unknown whether cell cycle retardation results in discrepancies regarding anti-melanogenic or melanogenic effects of pinostrobin, but future studies are needed.

Tyrosinase is a rate-limiting enzyme for melanin biosynthesis and contains copper ions at the catalytic center, which catalyze the hydroxylation and oxidation of substrates, including L-tyrosine and L-DOPA, to form dopachrome, resulting in melanin biosynthesis [30]. Therefore, many inhibitors targeting the catalytic center in tyrosinase have been developed [11,31,32]. In particular, many natural flavonoids fit into the catalytic pocket and are suitable chelators of Cu^{2+} using a flavonoid core and ionizable OH substituents. Hence, many flavonoids inhibit tyrosinase activity by competing with substrates at their catalytic site [33–35]. In this study, we demonstrated that pinostrobin inhibits mushroom tyrosinase activity *in vitro*, with an IC_{50} higher than that of flavonoids previously reported in other studies [36,37]. Molecular docking simulations confirmed the binding site of pinostrobin in tyrosinase. Unlike previously known flavonoids, pinostrobin does not fit into the active and catalytic centers, but rather binds primarily to another site between the light chain (lectin-like fold protein) and heavy chain (polyphenol oxidase). Whether this binding induces a conformational change in tyrosinase and acts as a non-competitive inhibitor is currently unknown. In addition, in order to accurately predict molecular docking between pinostrobin and tyrosinase, molecular dynamics and *in silico* molecular docking studies should be conducted.

Numerous cell signaling pathways are also involved in melanin biosynthesis. Among them, α -MSH-mediated upregulation of MITF is considered a key inducer of melanogenesis [38]. The binding of α -MSH to MC1R promotes cAMP formation and subsequently activates PKA-mediated CREB phosphorylation, which consequently transactivates MITF [13]. Activated MITF subsequently enhances the transcription of melanogenesis-promoting proteins such as tyrosinase [39]. Liu-Smith and Meyskens [40] previously reported that flavonoids inhibit melanin biosynthesis by suppressing the cAMP–PKA–CREB–MITF–tyrosinase signaling pathway, leading to excellent effects in the prevention and treatment of melanoma. In this study, we found that pinostrobin effectively inhibited α -MSH-mediated melanin biosynthesis, both *in vitro* and *in vivo*, by suppressing tyrosinase expression and activity. Unlike previous studies [36,41], pinostrobin effectively inhibits melanin biosynthesis in α -MSH-treated B16F10 melanoma cells and zebrafish larvae at 50 and 25 μM , respectively, which is relatively low compared with the IC_{50} (approximately 700 μM) of *in vitro* mushroom tyrosinase. These results suggest that pinostrobin exerts its effect predominantly via interference with the melanin biosynthesis cell signaling pathway rather than through direct inhibition of tyrosinase activity. Additionally, Pillaiyar et al. [42] reported that several soluble factors, such as wingless-related integration site, stem cell factor, and endothelin-1, stimulate MITF-mediated melanogenesis in melanocytes. Therefore, it is necessary to determine whether pinostrobin also contributes to the inhibition of other signaling pathways in addition to inhibiting the α -MSH-induced melanogenesis signaling process. Furthermore, we need to perform the more preclinical experiment to identify the physiological concentration of pinostrobin to inhibit α -MSH-induced melanogenesis.

4. Materials and Methods

4.1. Regents and Antibodies

Dulbecco's Modified Eagle's Medium (DMEM), fetal bovine serum (FBS), and an antibiotic mixture were purchased from WelGENE (Gyeongsan, Gyeongsangbuk-do, Re-

public of Korea). PTU, AA, KA, mushroom tyrosinase, 3-(4,5-dimethylthiazol-2-yl)-2,5-diphenyltetrazolium bromide (MTT), α -MSH, and 3-isobutyl-1-methylxanthine (IBMX) were purchased from Sigma-Aldrich (St. Louis, MO, USA). Antibodies against tyrosinase (sc-20035), MITF (sc-71588), p-CREB (sc-81486), and β -actin (sc-69879) were obtained from the Santa Cruz Biotechnology (Dallas, TX, USA). Pinostrobin (purity: $\geq 99\%$) was purified from the stems of *Prunus serrulata* Lindl. *F. serrulata spontanea* (Maxim.) Chin S. Chang according to a previous method [43] and was provided from the National Institute of Forest Science (Suwon, Gyeonggi-do, Republic of Korea). All other chemicals were purchased from Sigma-Aldrich.

4.2. In Vitro Mushroom Tyrosinase Assay

Tyrosinase inhibition was measured using mushroom tyrosinase in a cell-free system by modifying the method of Duckworth and Coleman [44]. Briefly, the reaction mixture was prepared with 130 μ L of 100 mM phosphate buffer (pH 6.8), 20 μ L of pinostrobin, 30 μ L of 1.5 mM L-tyrosine, and 20 μ L of 210 U/mL mushroom tyrosinase and incubated for 30 min at 37 °C, and absorbance was measured at 490 nm using a microplate spectrophotometer (Thermo Fisher Scientific, Rockford, IL, USA). PTU (250 nM), AA (500 μ M), and KA (25 μ M) were used as positive controls. The inhibition rate (%) of mushroom tyrosinase in vitro was calculated using Equation (1):

$$\text{Inhibition (\%)} = [A_0 - (A_1 - A_2)/A_0] - 100 \quad (1)$$

where A_0 , A_1 , and A_2 are the absorbance values of the control ((L-tyrosine + tyrosinase) – L-tyrosine), samples (L-tyrosine + samples + tyrosinase), and blank (L-tyrosine + samples), respectively. IC_{50} was calculated using GraphPad Prism 9.3 (San Diego, CA, USA).

4.3. Molecular Docking

The crystal structure of tyrosinase from *Agaricus bisporus* [protein database bank (PDB) ID: 2Y9X] was obtained from the RCSB PDB, and the chemical structure of pinostrobin (CID: 73201) was obtained from PubChem (<https://pubchem.ncbi.nlm.nih.gov>). For protein–ligand docking, simulations were performed using SwissDock (swissdockd_6tLCTN_0RI6WK5VODF69B6RFS4], accessed on 23 December 2022) [45]. A monomer of 2Y9X (a heavy (polyphenol oxidase) and a light (lectin-like fold protein) chain) was as the full structure of 2Y9X could not be uploaded to SwissDock. Molecular docking data were visualized using the UCSF Chimera. A 2D interaction diagram was constructed using Discovery Studio Visualizer (<https://www.discover.3ds.com/discovery-studio-visualizer-download>).

4.4. Cell Culture and Cell Viability Assay

Murine B16F10 melanoma cells (ATCC, Manassas, VA, USA) were maintained in DMEM supplemented with 10% heat-inactivated FBS at 37 °C in a humidified atmosphere containing 5% CO₂. To analyze the effect of pinostrobin on cell viability, an MTT assay was performed. Briefly, B16F10 melanoma cells were seeded in 24-well plates at a density of 1×10^4 cells/mL for 16 h. The cells were then treated with the indicated concentrations of pinostrobin (0–200 μ M) for 24, 48, and 72 h. After incubation, MTT was added to each well and the plates were incubated for 4 h at 37 °C. The precipitate was dissolved in dimethyl sulfoxide (DMSO), and the absorbance was measured at 540 nm using a microplate spectrophotometer (Thermo Fisher Scientific, Waltham, MA, USA). Cellular morphology was observed under a stereomicroscope (MACROTECH, Goyang, Gyeonggi-do, Republic of Korea).

4.5. Flow Cytometry Analysis

To estimate the total viable cell count and viable cell population, flow cytometry was performed. Briefly, B16F10 melanoma cells were plated at a density of 1×10^4 cells/mL and treated with the indicated concentrations of pinostrobin (0–200 μ M) for 72 h. Hydrogen

peroxide (H_2O_2 , 100 μM) was added for 24 h and used as a cell death-inducing control. Briefly, the cells were harvested and washed with ice-cold phosphate-buffered saline (PBS). The cells were then incubated with a Muse Cell Count and Viability Kit (Luminex, Austin, Texas, USA) for 5 min and analyzed using a Muse Cell Analyzer (Luminex).

4.6. Measurement of Extracellular and Intracellular Melanin Content

Melanin content was measured as previously described [46]. B16F10 melanoma cells were cultured at 1×10^4 cell/mL in 6-well plates for 16 h and treated with α -MSH (500 ng/mL) for 24 h, followed by treatment with the indicated concentrations of pinostrobin (0–50 μM) for 48 h. Extracellular melanin content was measured using culture media at 405 nm. To measure the intracellular melanin content, the cells were washed in ice-cold PBS and dissolved in 1 N NaOH containing 10% DMSO at 100 °C for 10 min. The dissolved melanin content was measured at 405 nm.

4.7. Measurement of Intracellular Tyrosinase Activity

Intracellular tyrosinase activity was measured as previously described [47]. Briefly, B16F10 melanoma cells (5×10^4 cells/mL) were pretreated with 500 ng/mL α -MSH for 24 h and the indicated concentrations of pinostrobin (0–50 μM) were incubated for 48 h. The cells were then lysed with PBS containing 1% Triton X-100 by freezing at -20 °C for 2 h and disrupted by thawing at room temperature. Total protein was quantified using Bio-Rad Protein Assay Reagents (Bio-Rad, Hercules, CA, USA) and an equal amount of protein was mixed with 90 μL of 5 mM L-DOPA at 37 °C for 30 min. Absorbance was measured at a wavelength of 405 nm.

4.8. Enzyme-Linked Immunosorbent Assay (ELISA) for cAMP

B16F10 melanoma cells (5×10^4 cells/mL) were cultured in serum-free DMEM media and pretreated with 1 mM IBMX for 10 min. Pinostrobin (0–50 μM) was then added in the presence or absence of 500 ng/mL α -MSH for 15 min. Intracellular cAMP levels were measured using a colorimetric ELISA kit (Cell Biolabs Inc., San Diego, CA, USA). Finally, the absorbance was measured at 450 nm and the amount of cAMP was calculated using a cAMP standard curve.

4.9. Reverse Transcription-Polymerase Chain Reaction (RT-PCR)

B16F10 melanoma cells were seeded at 1×10^4 cells/mL in 6-well plates and pretreated with α -MSH (500 ng/mL) 24 h before treatment with pinostrobin (0–50 μM) for 48 h. Total RNA was extracted using an easy-BLUE Total RNA Extraction Kit (iNtRON Biotechnology, Seongnam, Gyeonggi-do, Republic of Korea), according to the manufacturer's protocol. The sequences of the sense and antisense primers were as follows: tyrosinase (TYR) sense 5'-GTCGTCACCCTGAAAATCCTAACT-3' and antisense 5'-CATCGCATAAAACCTGATGGC-3'; MITF sense 5'-CCCGTCTCTGGAACTTGATCG-3' and antisense 5'-CTGTACTCTGAGCAGCAGGTC-3'; glyceraldehyde-3-phosphate dehydrogenase (GAPDH) sense 5'-AGGTCGGTGTGAACGGATTTG-3' and antisense 5'-TGTAGACCATGTAGTTGAGGTCA-3' [48]. PCR was conducted using a Veriti 96-well thermal cycler (Thermo Fisher Scientific). The PCR products were visualized using ethidium bromide.

4.10. Western Blot Analysis

B16F10 melanoma cells were seeded at a density of 1×10^4 cell/mL in 6-well plates. The cells were then pretreated with α -MSH (500 ng/mL) for 24 h before treatment with pinostrobin (0–50 μM) for 48 h and subsequently lysed using PRO-PREP lysis buffer (iNtRON Biotechnology). The supernatant was collected, and protein concentrations were measured using Bio-Rad protein assay reagents (Bio-Rad). Equal amounts of protein (25 μg) were separated on SDS-polyacrylamide gels, transferred to nitrocellulose membranes (Schleicher & Schuell, Keene, NH, USA), and immunoblotted with specific antibodies. The

bound antibodies were detected using an enhanced chemiluminescence plus kit (Thermo Fisher Scientific). Images were visualized and captured using ImageQuant LAS 500 (GE Healthcare Bio-Sciences AB, Uppsala, Sweden).

4.11. Maintenance of Zebrafish

AB strain zebrafish were provided by C.H. Kang (Nakdong National Institute of Biological Resources, Sangju, Gyeongsangbuk-do, Republic of Korea) and cultured at 28 °C under a 14/10 h light/dark cycle. Zebrafish were handled according to the standard guidelines of the Animal Care and Use Committee of Jeju National University (approval No. 2022-0036). Zebrafish housing and husbandry was followed by the recommendations [49]. Embryos obtained from natural spawning in embryo medium [34.8 g NaCl, 1.6 g KCl, 5.8 g CaCl₂·2H₂O, and 9.78 g MgCl₂·6H₂O in double-distilled water, pH 7.2]. The media was supplemented with 1% methylene blue at 28 °C.

4.12. Melanogenesis and Heart Rate in Zebrafish

One day post-fertilization (dpf) zebrafish larvae ($n = 20$) were pretreated with PTU (200 µM) for 48 h and then incubated with α -MSH (1 µg/mL) for an additional 24 h. At 4 dpf, the medium was replaced with PTU and α -MSH, and the embryos were treated with pinostrobin (0–25 µM) for 48 h (at 6 dpf). After anesthetizing zebrafish larvae with 0.02% tricane methanesulfonate, they were mounted in 2% methyl cellulose on a depression slide, and images were collected using stereomicroscopy (Tokyo, Japan). Densitometric analysis was performed using the ImageJ software (National Institutes of Health, Bethesda, MA, USA). The quantification of pigmentation data was calculated as a percentage of untreated zebrafish larvae. In a parallel experiment, heart rate was manually calculated using a stereomicroscope. The results are represented as the average heart rate per minute.

4.13. Statistical Analysis

All data in this study represent the mean of triplicate experiments and are expressed as mean \pm standard error (SE). Statistical analysis was performed using Sigma plot 12.0 (Systat Software Inc., San Jose, CA, USA) by Student's *t*-test and unpaired one-way analysis of variance (ANOVA) with Bonferroni's correction.

5. Conclusions

In conclusion, this study demonstrates that pinostrobin potently inhibits melanin biosynthesis *in vitro* and *in vivo*, thus eliciting a significant anti-melanogenic effect (Figure 7). This suggests that pinostrobin has the potential for novel clinical applications in the prevention and treatment of dermatological disorders, including wrinkling, melasma, and senile lentigines.

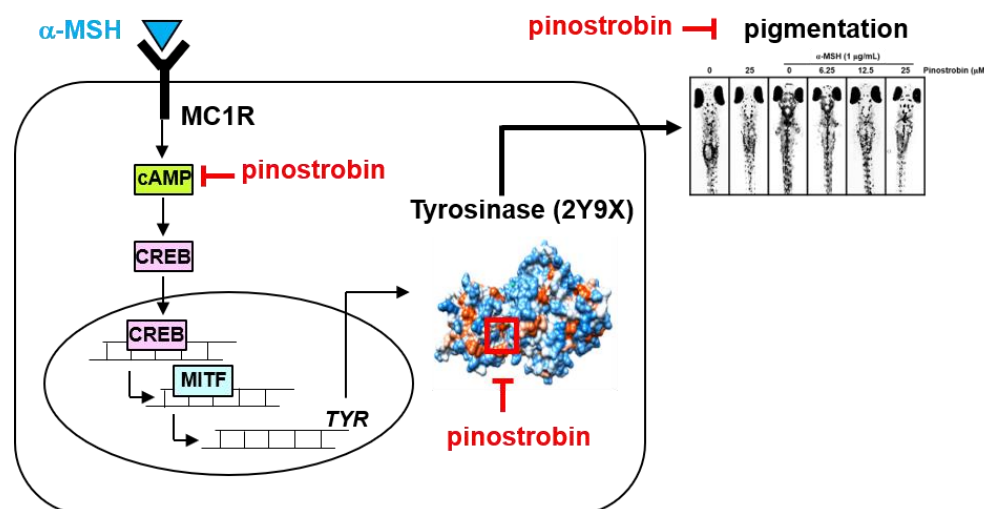


Figure 7. A scheme showing the molecular action of pinostrobin in inhibiting melanogenesis.

Supplementary Materials: The supporting information can be downloaded at: <https://www.mdpi.com/article/10.3390/ijms24010821/s1>.

Author Contributions: A.M.G.K.A.: Conceptualization, Methodology, Investigation, Validation, Visualization, Writing—original draft. S.S.S.: Conceptualization, Methodology, Investigation, Validation, Visualization, Writing—original draft. K.T.L.: Conceptualization, Resources, Methodology, Investigation. W.A.H.M.K.: Conceptualization, Visualization, Validation. Y.H.C.: Writing—review & editing. S.-P.H.: Conceptualization, Investigation, Visualization, Validation, Writing—review & editing. G.-Y.K.: Conceptualization, Visualization, Validation, Supervision, Writing—review & editing. All authors have read and agreed to the published version of the manuscript.

Funding: This research was supported by the 2022 scientific promotion program funded by Jeju National University.

Institutional Review Board Statement: The animal experiment was approved by Animal Care and Use Committee of Jeju National University (Jeju Special Self-governing Province, Republic of Korea; permission no. and date: 2022-0036, 9 June 2022). All experimental procedures were carried out in accordance with the approved.

Informed Consent Statement: Not applicable.

Data Availability Statement: All data analyzed in this study are available from the corresponding author (immunkim@jejunu.ac.kr) on reasonable request.

Conflicts of Interest: All authors declare that there is no conflict of interest.

References

- Ohbayashi, N.; Fukuda, M. Recent advances in understanding the molecular basis of melanogenesis in melanocytes. *F1000Research* **2020**, *9*, 608. [\[CrossRef\]](#)
- Solano, F. Photoprotection and skin pigmentation: Melanin-related molecules and some other new agents obtained from natural sources. *Molecules* **2020**, *25*, 1537. [\[CrossRef\]](#) [\[PubMed\]](#)
- Cestari, T.F.; Dantas, L.P.; Boza, J.C. Acquired hyperpigmentations. *An. Bras. Dermatol.* **2014**, *89*, 11–25. [\[CrossRef\]](#) [\[PubMed\]](#)
- Fistarol, S.K.; Itin, P.H. Disorders of pigmentation. *J. Dtsch. Dermatol. Ges.* **2010**, *8*, 187–201, quiz 201–2. [\[CrossRef\]](#)
- Cabaco, L.C.; Tomas, A.; Pojo, M.; Barral, D.C. The dark side of melanin secretion in cutaneous melanoma aggressiveness. *Front. Oncol.* **2022**, *12*, 887366. [\[CrossRef\]](#)
- Goelzer Neto, C.F.; do Nascimento, P.; da Silveira, V.C.; de Mattos, A.B.N.; Bertol, C.D. Natural sources of melanogenic inhibitors: A systematic review. *Int. J. Cosmet. Sci.* **2022**, *44*, 143–153. [\[CrossRef\]](#)
- Qian, W.; Liu, W.; Zhu, D.; Cao, Y.; Tang, A.; Gong, G.; Su, H. Natural skin-whitening compounds for the treatment of melanogenesis (Review). *Exp. Ther. Med.* **2020**, *20*, 173–185. [\[CrossRef\]](#)
- Sohretoglu, D.; Sari, S.; Barut, B.; Ozel, A. Tyrosinase inhibition by some flavonoids: Inhibitory activity, mechanism by in vitro and in silico studies. *Bioorg. Chem.* **2018**, *81*, 168–174. [\[CrossRef\]](#)

9. Nazir, Y.; Rafique, H.; Roshan, S.; Shamas, S.; Ashraf, Z.; Rafiq, M.; Tahir, T.; Qureshi, Z.U.; Aslam, A.; Asad, M. Molecular docking, synthesis, and tyrosinase inhibition activity of acetophenone amide: Potential inhibitor of melanogenesis. *Biomed. Res. Int.* **2022**, *2022*, 1040693. [[CrossRef](#)]
10. Noh, H.; Lee, S.J.; Jo, H.J.; Choi, H.W.; Hong, S.; Kong, K.H. Histidine residues at the copper-binding site in human tyrosinase are essential for its catalytic activities. *J. Enzyme Inhib. Med. Chem.* **2020**, *35*, 726–732. [[CrossRef](#)]
11. Goldfeder, M.; Kanteev, M.; Isaschar-Ovdat, S.; Adir, N.; Fishman, A. Determination of tyrosinase substrate-binding modes reveals mechanistic differences between type-3 copper proteins. *Nat. Commun.* **2014**, *5*, 4505. [[CrossRef](#)] [[PubMed](#)]
12. Oren, M.; Bartek, J. The sunny side of p53. *Cell* **2007**, *128*, 826–828. [[CrossRef](#)] [[PubMed](#)]
13. Garcia-Borron, J.C.; Abdel-Malek, Z.; Jimenez-Cervantes, C. MC1R, the cAMP pathway, and the response to solar UV: Extending the horizon beyond pigmentation. *Pigment Cell Melanoma Res.* **2014**, *27*, 699–720. [[CrossRef](#)] [[PubMed](#)]
14. Zhou, S.; Zeng, H.; Huang, J.; Lei, L.; Tong, X.; Li, S.; Zhou, Y.; Guo, H.; Khan, M.; Luo, L.; et al. Epigenetic regulation of melanogenesis. *Ageing Res. Rev.* **2021**, *69*, 101349. [[CrossRef](#)]
15. Jones, A.A.; Gehler, S. Acacetin and pinostrobin inhibit malignant breast epithelial cell adhesion and focal adhesion formation to attenuate cell migration. *Integr. Cancer Ther.* **2020**, *19*, 1534735420918945. [[CrossRef](#)]
16. Jadaun, A.; Sharma, S.; Verma, R.; Dixit, A. Pinostrobin inhibits proliferation and induces apoptosis in cancer stem-like cells through a reactive oxygen species-dependent mechanism. *RSC Adv.* **2019**, *9*, 12097–12109. [[CrossRef](#)]
17. Wu, N.; Fu, K.; Fu, Y.J.; Zu, Y.G.; Chang, F.R.; Chen, Y.H.; Liu, X.L.; Kong, Y.; Liu, W.; Gu, C.B. Antioxidant activities of extracts and main components of pigeonpea [*Cajanus cajan* (L.) Millsp.] leaves. *Molecules* **2009**, *14*, 1032–1043. [[CrossRef](#)]
18. Athapaththu, A.; Lee, K.T.; Kavinda, M.H.D.; Lee, S.; Kang, S.; Lee, M.H.; Kang, C.H.; Choi, Y.H.; Kim, G.Y. Pinostrobin ameliorates lipopolysaccharide (LPS)-induced inflammation and endotoxemia by inhibiting LPS binding to the TLR4/MD2 complex. *Biomed. Pharmacother.* **2022**, *156*, 113874. [[CrossRef](#)]
19. Gonzalez, A.S.; Soto Tellini, V.H.; Benjumea Gutierrez, D.M. Study of the dermal anti-inflammatory, antioxidant, and analgesic activity of pinostrobin. *Heliyon* **2022**, *8*, e10413. [[CrossRef](#)]
20. Bahadur Gurung, A.; Ajmal Ali, M.; Al-Hemaid, F.; El-Zaidy, M.; Lee, J. In silico analyses of major active constituents of fingerroot (*Boesenbergia rotunda*) unveils inhibitory activities against SARS-CoV-2 main protease enzyme. *Saudi. J. Biol. Sci.* **2022**, *29*, 65–74. [[CrossRef](#)]
21. El-Nashar, H.A.S.; El-Din, M.I.G.; Hritcu, L.; Eldahshan, O.A. Insights on the inhibitory power of flavonoids on tyrosinase activity: A survey from 2016 to 2021. *Molecules* **2021**, *26*, 7546. [[CrossRef](#)] [[PubMed](#)]
22. Cichorek, M.; Wachulska, M.; Stasiewicz, A.; Tyminska, A. Skin melanocytes: Biology and development. *Postepy Dermatol. Alergol.* **2013**, *30*, 30–41. [[CrossRef](#)] [[PubMed](#)]
23. Napolitano, A.; Panzella, L.; Monfrecola, G.; d'Ischia, M. Pheomelanin-induced oxidative stress: Bright and dark chemistry bridging red hair phenotype and melanoma. *Pigment Cell Melanoma Res.* **2014**, *27*, 721–733. [[CrossRef](#)]
24. Lee, A.Y. Skin pigmentation abnormalities and their possible relationship with skin aging. *Int. J. Mol. Sci.* **2021**, *22*, 3727. [[CrossRef](#)] [[PubMed](#)]
25. Yamaguchi, Y.; Hearing, V.J. Melanocytes and their diseases. *Cold Spring Harb. Perspect. Med.* **2014**, *4*, a017046. [[CrossRef](#)]
26. Zolghadri, S.; Bahrami, A.; Hassan Khan, M.T.; Munoz-Munoz, J.; Garcia-Molina, F.; Garcia-Canovas, F.; Saboury, A.A. A comprehensive review on tyrosinase inhibitors. *J. Enzyme Inhib. Med. Chem.* **2019**, *34*, 279–309. [[CrossRef](#)]
27. Patel, N.K.; Jaiswal, G.; Bhutani, K.K. A review on biological sources, chemistry and pharmacological activities of pinostrobin. *Nat. Prod. Res.* **2016**, *30*, 2017–2027. [[CrossRef](#)]
28. Yoon, J.H.; Youn, K.; Jun, M. Discovery of pinostrobin as a melanogenic agent in cAMP/PKA and p38 MAPK signaling pathway. *Nutrients* **2022**, *14*, 3713. [[CrossRef](#)]
29. Jaudan, A.; Sharma, S.; Malek, S.N.A.; Dixit, A. Induction of apoptosis by pinostrobin in human cervical cancer cells: Possible mechanism of action. *PLoS ONE* **2018**, *13*, e0191523. [[CrossRef](#)]
30. Solano, F. On the metal cofactor in the tyrosinase family. *Int. J. Mol. Sci.* **2018**, *19*, 633. [[CrossRef](#)]
31. Rolff, M.; Schottenheim, J.; Decker, H.; Tuzcek, F. Copper-O₂ reactivity of tyrosinase models towards external monophenolic substrates: Molecular mechanism and comparison with the enzyme. *Chem. Soc. Rev.* **2011**, *40*, 4077–4098. [[CrossRef](#)] [[PubMed](#)]
32. Favre, E.; Daina, A.; Carrupt, P.A.; Nurisso, A. Modeling the met form of human tyrosinase: A refined and hydrated pocket for antagonist design. *Chem. Biol. Drug Des.* **2014**, *84*, 206–215. [[CrossRef](#)] [[PubMed](#)]
33. Jakimiuk, K.; Sari, S.; Milewski, R.; Supuran, C.T.; Sohretoglu, D.; Tomczyk, M. Flavonoids as tyrosinase inhibitors in in silico and in vitro models: Basic framework of SAR using a statistical modelling approach. *J. Enzyme Inhib. Med. Chem.* **2022**, *37*, 421–430. [[CrossRef](#)] [[PubMed](#)]
34. Arroo, R.R.J.; Sari, S.; Barut, B.; Ozel, A.; Ruparelia, K.C.; Sohretoglu, D. Flavones as tyrosinase inhibitors: Kinetic studies in vitro and in silico. *Phytochem. Anal.* **2020**, *31*, 314–321. [[CrossRef](#)] [[PubMed](#)]
35. Li, X.; Guo, J.; Lian, J.; Gao, F.; Khan, A.J.; Wang, T.; Zhang, F. Molecular simulation study on the interaction between tyrosinase and flavonoids from sea buckthorn. *ACS Omega* **2021**, *6*, 21579–21585. [[CrossRef](#)]
36. Obaid, R.J.; Mughal, E.U.; Naeem, N.; Sadiq, A.; Alsantali, R.I.; Jassas, R.S.; Moussa, Z.; Ahmed, S.A. Natural and synthetic flavonoid derivatives as new potential tyrosinase inhibitors: A systematic review. *RSC Adv.* **2021**, *11*, 22159–22198. [[CrossRef](#)]

37. Promden, W.; Viriyabancha, W.; Monthakantirat, O.; Umehara, K.; Noguchi, H.; De-Eknamkul, W. Correlation between the potency of flavonoids on mushroom tyrosinase inhibitory activity and melanin synthesis in melanocytes. *Molecules* **2018**, *23*, 1403. [[CrossRef](#)]
38. Kawakami, A.; Fisher, D.E. The master role of microphthalmia-associated transcription factor in melanocyte and melanoma biology. *Lab. Investig.* **2017**, *97*, 649–656. [[CrossRef](#)]
39. Hida, T.; Kamiya, T.; Kawakami, A.; Ogino, J.; Sohma, H.; Uhara, H.; Jimbow, K. Elucidation of melanogenesis cascade for identifying pathophysiology and therapeutic approach of pigmentary disorders and melanoma. *Int. J. Mol. Sci.* **2020**, *21*, 6129. [[CrossRef](#)]
40. Liu-Smith, F.; Meyskens, F.L. Molecular mechanisms of flavonoids in melanin synthesis and the potential for the prevention and treatment of melanoma. *Mol. Nutr. Food Res.* **2016**, *60*, 1264–1274. [[CrossRef](#)]
41. Abbas, Q.; Ashraf, Z.; Hassan, M.; Nadeem, H.; Latif, M.; Afzal, S.; Seo, S.Y. Development of highly potent melanogenesis inhibitor by in vitro, in vivo and computational studies. *Drug Des. Devel. Ther.* **2017**, *11*, 2029–2046. [[CrossRef](#)] [[PubMed](#)]
42. Pillaiyar, T.; Manickam, M.; Jung, S.H. Recent development of signaling pathways inhibitors of melanogenesis. *Cell. Signal.* **2017**, *40*, 99–115. [[CrossRef](#)] [[PubMed](#)]
43. Smolarz, H.D.; Mendyk, E.; Bogucka-Kocka, A.; Kocki, J. Pinostrobin—an anti-leukemic flavonoid from *Polygonum lapathifolium* L. ssp. nodosum (Pers.) Dans. *Z. Naturforsch. C. J. Biosci.* **2006**, *61*, 64–68. [[CrossRef](#)] [[PubMed](#)]
44. Duckworth, H.W.; Coleman, J.E. Physicochemical and kinetic properties of mushroom tyrosinase. *J. Biol. Chem.* **1970**, *245*, 1613–1625. [[CrossRef](#)] [[PubMed](#)]
45. Bitencourt-Ferreira, G.; de Azevedo, W.F., Jr. Docking with SwissDock. *Methods Mol. Biol.* **2019**, *2053*, 189–202.
46. Hseu, Y.C.; Vudhya Gowrisankar, Y.; Wang, L.W.; Zhang, Y.Z.; Chen, X.Z.; Huang, P.J.; Yen, H.R.; Yang, H.L. The in vitro and in vivo depigmenting activity of pterostilbene through induction of autophagy in melanocytes and inhibition of UVA-irradiated alpha-MSH in keratinocytes via Nrf2-mediated antioxidant pathways. *Redox Biol.* **2021**, *44*, 102007. [[CrossRef](#)]
47. Chung, S.; Lim, G.J.; Lee, J.Y. Quantitative analysis of melanin content in a three-dimensional melanoma cell culture. *Sci. Rep.* **2019**, *9*, 780. [[CrossRef](#)]
48. Molagoda, I.M.N.; Kavinda, M.H.D.; Ryu, H.W.; Choi, Y.H.; Jeong, J.W.; Kang, S.; Kim, G.Y. Gamma-Aminobutyric Acid (GABA) Inhibits α -melanocyte-stimulating hormone-induced melanogenesis through GABA_A and GABA_B receptors. *Int. J. Mol. Sci.* **2021**, *22*, 8257. [[CrossRef](#)]
49. Alestrom, P.; D'Angelo, L.; Midtlyng, P.J.; Schorderet, D.F.; Schulte-Merker, S.; Sohm, F.; Warner, S. Zebrafish: Housing and husbandry recommendations. *Lab. Anim.* **2020**, *54*, 213–224. [[CrossRef](#)]

Disclaimer/Publisher's Note: The statements, opinions and data contained in all publications are solely those of the individual author(s) and contributor(s) and not of MDPI and/or the editor(s). MDPI and/or the editor(s) disclaim responsibility for any injury to people or property resulting from any ideas, methods, instructions or products referred to in the content.